Selective Oxidative Dehydrogenation of Ethane and Propane over Copper-Containing Mordenite: Insights into Reaction Mechanism and Product Protection

Originally published in:
Angewandte Chemie. International Edition 62(44), https://doi.org/10.1002/anie.202309180

Funding acknowledgement:
178943 - Catalyst structures in three dimensions (SNF)

How to cite: *Angew. Chem. Int. Ed.* **2023**, *62*, e202309180
doi.org/10.1002/anie.202309180

Hetereogeneous Catalysis

Selective Oxidative Dehydrogenation of Ethane and Propane over Copper-Containing Mordenite: Insights into Reaction Mechanism and Product Protection

Mikalai A. Artsiusheuski, René Verel, Jeroen A. van Bokhoven, and Vitaly L. Sushkevich**

Abstract: Copper(II)-containing mordenite (CuMOR) is capable of activation of C–H bonds in C_1-C_3 alkanes, albeit there are remarkable differences between the functionalization of ethane and propane compared to methane. The reaction of ethane and propane with CuMOR results in the formation of ethylene and propylene, while the reaction of methane predominantly yields methanol and dimethyl ether. By combining in situ FTIR and MAS NMR spectroscopies as well as time-resolved Cu K-edge X-ray absorption spectroscopy, the reaction mechanism was derived, which differs significantly for each alkane. The formation of ethylene and propylene proceeds via oxidative dehydrogenation of the corresponding alkanes with selectivity above 95 % for ethane and above 85 % for propane. The formation of stable π-complexes of olefins with Cu^{I} sites, formed upon reduction of Cu^{II}-oxo species, protects olefins from further oxidation and/or oligomerization. This is different from methane, the activation of which proceeds via oxidative hydroxylation leading to the formation of surface methoxy species bonded to the zeolite framework. Our findings constitute one of the major steps in the direct conversion of alkanes to important commodities and open a novel research direction aiming at the selective synthesis of olefins.

Introduction

Alkanes are major components of natural gas and oil and therefore are inexpensive feedstocks for the chemical industry. However, there are very few processes for the direct valorization of alkanes. Low reactivity of alkanes arises from the localized C–H and C–C bonds and the absence of low-energy empty or high-energy occupied orbitals.[1,2] Therefore, the main industrial processes for the transformation of alkanes, especially the least reactive light ones, to valuable commodities are indirect and consist of several stages.

The valorization of methane, which is a main component of natural gas,[3] relies on syngas-based processes. First, methane is converted to a mixture of carbon monoxide and hydrogen by steam reforming,[4] the resulting syngas is utilized for the production of fuels[5] and/or chemicals.[6] The first stage of steam reforming is extremely energy-extensive and is feasible only on a large scale,[7] causing flaring of substantial amounts of methane from associated petroleum gas at scattered and remote oil fields.[8] This urges the development of energy-efficient small-scale processes for methane direct valorization to the transportable commodities.

After methane, ethane and propane are the largest components of natural gas.[3] The chief method for their valorization is steam cracking.[9] This process requires temperatures above 1000 K, and is energetically inefficient.[10] Moreover, while for ethane the selectivity towards ethylene is high, steam cracking of propane is much less selective and leads to the formation of a mixture of hydrocarbons containing methane, ethylene, propylene and aromatics.[9] For propane conversion to propylene alternative approaches are implemented, in particular, non-oxidative and oxidative dehydrogenation.[11,12] However, these processes have drawbacks: the former demonstrates low conversion and requires temperatures above 773 K due to thermodynamic limitations, while the latter suffers from overoxidation of the desired olefin due to its higher reactivity as compared to alkane.[13] Given that the global demands for ethylene and propylene are continuously growing,[14] novel technologies for the direct, energy-efficient and selective transformations of ethane and propane to olefins are of enormous interest.

A promising route for the valorization of methane is the direct oxidation to methanol over copper-containing zeolites in a three-step process, also referred to as chemical

[*] M. A. Artsiusheuski, R. Verel, J. A. van Bokhoven
Institute for Chemistry and Bioengineering, ETH Zurich
Vladimir-Prelog-Weg 1, 8093 Zurich (Switzerland)
E-mail: jeroen.vanbokhoven@chem.ethz.ch
M. A. Artsiusheuski, J. A. van Bokhoven, V. L. Sushkevich
Laboratory for Catalysis and Sustainable Chemistry,
Paul Scherrer Institut
5232 Villigen PSI (Switzerland)
E-mail: vitaly.sushkevich@psi.ch

looping.[15–17] The first step is activation of copper-containing zeolite in oxidative environment at temperature 673 K or higher, resulting in the formation of copper(II)-oxo species.[18,19] In the case of the widely utilized copper-containing MOR[20–22] zeolite most favorable centers are mono-μ-oxo dicopper(II) sites. The second stage is the reaction between activated material and methane. This step is generally carried out at a temperature of 473 K, and copper(II)-oxo sites convert methane to reaction products.[23–26] Simultaneously, copper(II)-oxo sites are reduced to copper(I) species.[20,27,28] Finally, the products of partial oxidation are converted to methanol by hydrolysis.[29]

While the activation of methane over copper-containing zeolites has been studied in depth, much less attention has been paid to C–H bond activation in other hydrocarbons. Recent studies show that copper-containing zeolites are potentially capable of the conversion of C_{2+} alkanes to corresponding olefins. As was shown by means of FTIR spectroscopy, the reaction of propane with copper-containing MFI zeolite at 573 K leads to the formation of a small amount of adsorbed propylene.[30] Later on, it was demonstrated that copper-containing MOR enables ethane conversion to ethylene in a stepwise process.[31] While several attempts have been made to tackle the problem of C_{2+} alkane activation over copper-containing zeolites, the most important questions remain and require careful examination. First, the mechanism of alkane transformation to olefin is unclear, and yet this is of utmost importance both for the fundamental understanding of the reaction and for the design of better-performing materials. Second, a pathway of alkene protection,[32] which prevents it from further oxidation is not known. Third, the nature of the reaction intermediates and the structure of the by-products is still to be studied. Next, the fate of copper(II)-oxo species upon the reduction with C_{2+} alkanes has never been analyzed. In addition, the effect of the reaction conditions, in particular the reaction temperature, is not studied yet. And this is essential for yield optimization and understanding the theoretical limits of a novel process.[33,34] And finally, the recyclability of the copper-containing zeolites for the stepwise activation of propane has never been demonstrated.

In this contribution, we address, in a systematic fashion, all of the above-mentioned points. We studied the transformation of ethane and propane over oxygen-activated copper(II)-containing mordenite using the chemical looping protocol and compared it to methane activation. By means of in situ FTIR and in situ MAS NMR spectroscopies we demonstrated that the primary products of ethane and propane reacting with copper(II)-oxo species are π-complexes of olefins with copper(I) centers. This is in contrast to methane oxidation, which leads to surface methoxy species bonded to the zeolite framework. The strong adsorption of ethylene and propylene hinders their oxidation, enabling selectivity above 95 % for ethylene and above 85 % for propylene formation. Upon contact with water vapor, these stabilized olefins desorb, thereby closing the looping cycle and launching the next one after consecutive activation. Time-resolved in situ Cu K-edge spectroscopy shows an order of magnitude faster C–H bond activation rate for ethane and propane compared to methane. At the same time, the apparent activation energy in the case of methane is 10 $kJ\,mol^{-1}$ lower. The mechanism for C–H bond activation in ethane and propane over copper-containing zeolites is oxidative dehydrogenation, while in the case of methane activation, oxidative hydroxylation takes place.

Results and Discussion

Copper-containing mordenite with a Si/Al ratio of 6 and a Cu/Al ratio of 0.38 denoted as "CuMOR"[35,36] was employed for the reaction with methane, ethane and propane using the chemical looping approach. The reaction protocol is provided in Section 1.5 of the Supporting Information. The characterization of the material (chemical composition, results of nitrogen physisorption and XRD patterns) is presented in Table S1 and Figure S2.

Figure 1 shows the profiles of the concentrations of the products in the gas phase during the desorption step after the reaction of methane (A) ethane (B) and propane (C) with CuMOR at 423 K. Different products are formed. The conversion of methane (Figure 1A) results in the formation of methanol and dimethyl ether, i.e. the products of methane oxidative hydroxylation, as reported in previous publications.[15,20,26,37,38] Apart from that, the overoxidation of methane takes place, resulting in the formation of carbon dioxide. In contrast to methane transformation to its alcohol, ethane and propane are transformed into the corresponding olefins, and no alcohols were found as reaction products. Apart from the formation of olefins, a minor extent of overoxidation to carbon dioxide was detected. Four consecutive reaction cycles show the stable productivity and selectivity towards ethylene and propylene (Figure S3).

Figures 1D–F and Table S2 summarize the effect of the reaction temperature on the amount of products formed in the reaction of CuMOR with methane, ethane and propane. There are remarkable differences between the activation of ethane and propane as compared to methane. First, the reaction temperature required for the formation of a similar amount of reaction products ($\approx$120 $\mu mol\cdot g^{1}$) changes as follows: CH_4 (453 K) > C_2H_6 (393 K) $\approx$ C_3H_8 (393 K). This clearly indicates that a lower temperature is required for ethane and propane activation than for methane. The similar reaction temperature for ethane and propane suggests that the reactivity does not scale linearly with the C–H bond strength.[39] For all substrates an increase in the reaction temperature leads to an increase in the amount of both partial and overoxidation products, indicating greater involvement of copper(II) sites in the reaction. Second, the impact of the reaction temperature on the selectivity is different. In the case of ethane and propane, the selectivity towards ethylene and propylene accounts for $\approx$95 % and $\approx$85 %, respectively, slightly trending upwards in the employed temperature range. We suggest that the formation of carbon dioxide might be associated with a non-ideal desorption protocol rather than with the intrinsic over-

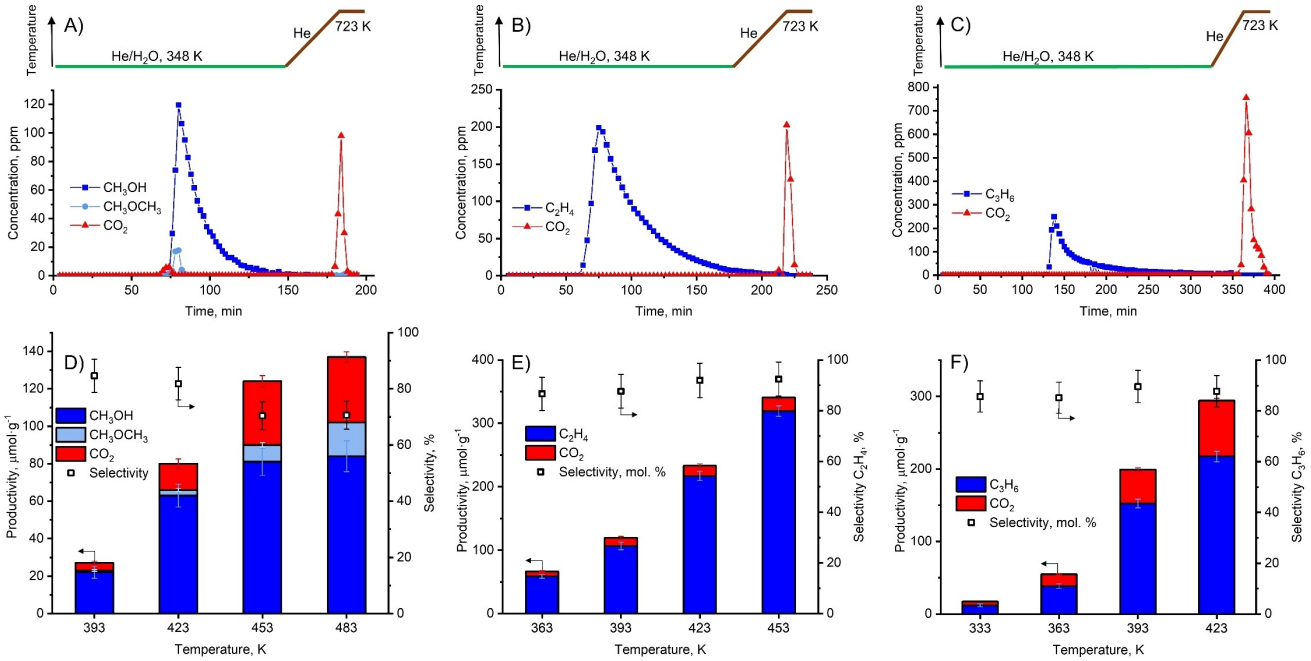

Figure 1. Concentration profiles of the products in the gas phase during the desorption step after the reaction of methane (A), ethane (B) and propane (C) with CuMOR at 423 K. Yields of products obtained in conversion of methane (D), ethane (E) and propane (F) over CuMOR at different reaction temperatures.

oxidation of C_{2+} alkanes. The reaction products, incompletely desorbed during the low temperature dwell (Figure 1B and C, green lines), undergo oxidation to CO_2 during the temperature ramp (ibid, brown line). The oxidant might be represented by unreacted copper(II)-oxo species or water.[35] In the case of methane conversion, the selectivity towards methanol decreases from 84 % at 393 K to 75 % at 483 K. A similar trend was observed for CuCHA zeolite,[38] and in our recent study we showed that this is associated with the decomposition of the methanol precursors and their further oxidation over copper(II) sites at elevated temperatures.[26]

In the next step, we followed the fate of each alkane in the course of conversion over CuMOR and identified the reaction intermediates by means of in situ FTIR and solid-state MAS NMR spectroscopies.[24–26] Figures 2A–C show the FTIR spectra of surface species formed during the conversion of methane, ethane and propane, respectively, over CuMOR. Table S3 lists the assignment of the signals.

The spectra corresponding to the surface species formed in the reaction of methane[24] contain intense bands centered at 2980, 2871 and 1458 cm^{-1}, which are due to C–H vibrations in the methoxy species attached to the zeolite framework[24,35,40–43] (Scheme 1A). The weaker bands at 2967, 2856 and 1469 cm^{-1} are associated with molecularly adsorbed methanol.[24,35,40–43] These species are products of methane partial oxidation and are precursors of methanol and DME formed upon contact with water vapor during the desorption step. The intensity of these bands increases with increasing reaction temperature up to 548 K due to the greater involvement of copper(II)-oxo sites. Additionally, the spectra corresponding to reaction temperatures between 448 K and 498 K possess bands at 2942, 2836, 1696, 1685 and 1491 cm^{-1} due to formaldehyde[24,44] and bands at 1632, 1619 and 1594 cm^{-1}, which are overlapping signals from the surface formate species[24,45] and adsorbed water.[24,45,46] These signals correspond to products of methane deeper oxidation, forming carbon dioxide in the reactor tests. Finally, the band at 2159 cm^{-1} corresponding to copper(I) carbonyl

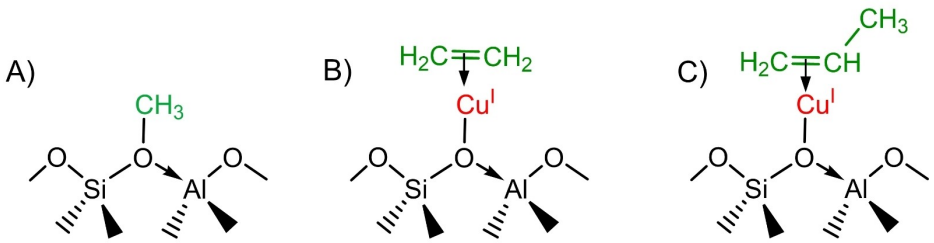

Scheme 1. Primary surface species formed after reaction of oxygen-activated CuMOR with methane (A), ethane (B) and propane (C).

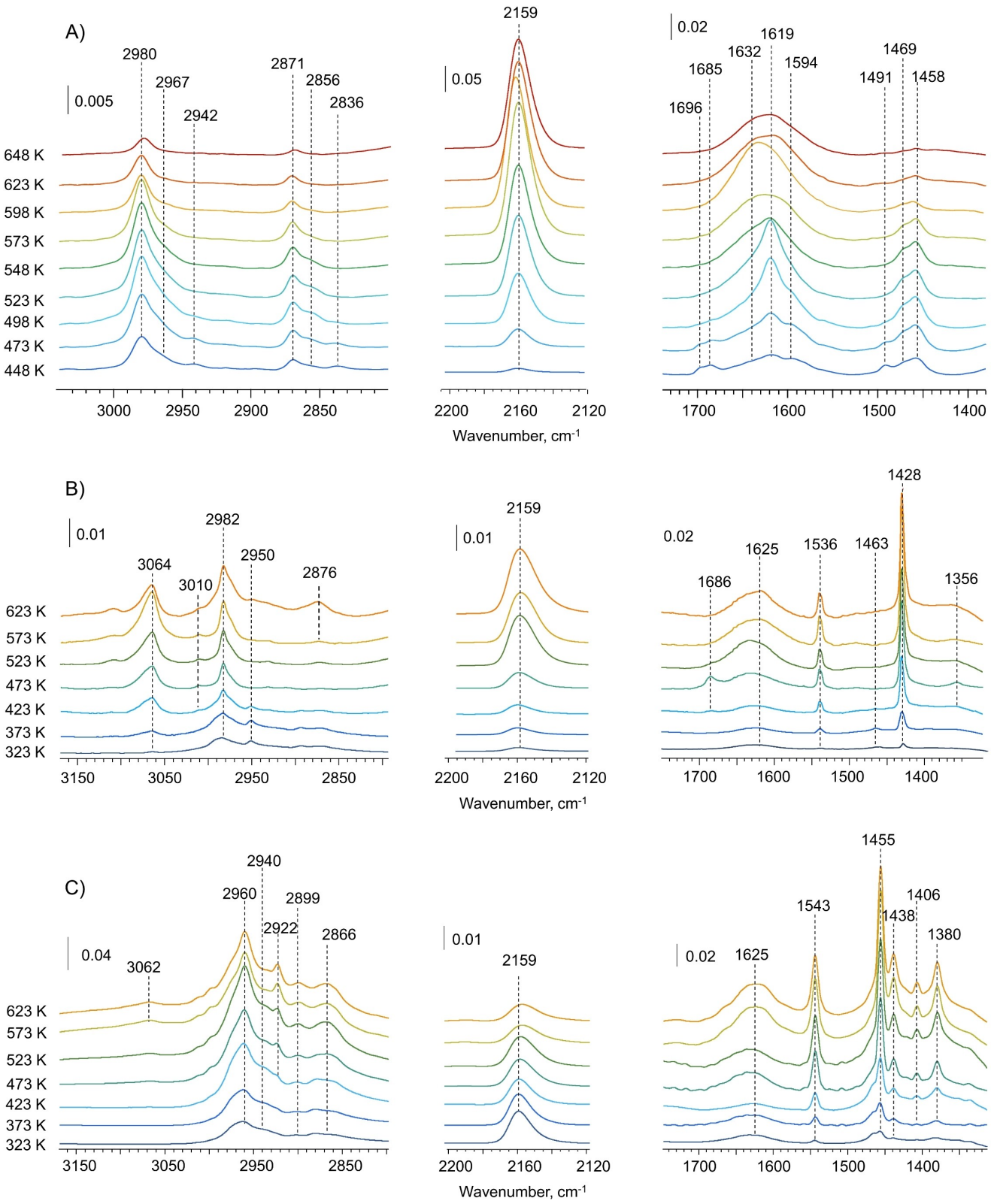

Figure 2. FTIR spectra of surface species formed after the reaction of oxygen-activated CuMOR with 285 Torr of methane (A),[24] ethane (B) and propane (C) for 5 min. Presented spectra are subtraction results obtained as difference between the spectrum after the reaction and subsequent evacuation of the gas phase at ambient temperature up to residual pressure of 3×10^{-6} Torr and the spectrum of the oxygen-activated CuMOR prior to the reaction.

species[24,47] appears in the spectra at 473 K and develops with increasing temperature. Employing attenuation coefficient for copper(I) carbonyl species recently reported by Deplano et al.,[48] we quantified their amount (Table S5). Importantly, the fraction of copper(I) carbonyl species does not exceed 7 % of the total copper sites even for the highest reaction temperature, which is in line with high methanol selectivity obtained in the reactor tests. An increase in the reaction temperature above 548 K leads to the decrease in the intensity of the IR bands corresponding to methane partial oxidation products. This points to their conversion and/or decomposition,[24,26] in agreement with the decrease in methanol selectivity in the reactor tests (Figure 1A).

Figure 2B demonstrates spectra of surface species observed after the reaction of ethane over CuMOR. All the spectra show bands at 3064, 3010, 2982 and 2876 cm^{-1} due to C–H stretching vibrations, the band at 1536 cm^{-1} due to the C=C stretching vibration and the band at 1428 cm^{-1} is associated with the $=CH_2$ scissoring vibration characteristic for ethylene.[49–51] The frequencies indicate that ethylene is adsorbed over copper(I) sites rather than over Brønsted acid sites, extra-framework aluminum species, or silanol groups[49–51] (Scheme 1B). The broad band at 1625 cm^{-1} is due to adsorbed water.[24,45] The intensity of the bands increases with the reaction temperature, indicating progressive conversion of ethane to ethylene, in line with the results of the reactor tests. Notably, ethylene is strongly bonded to copper(I) sites formed upon reduction of copper(II) species; no loss of signal intensity is observed even at 623 K. The spectra also contain a weak signal at 2159 cm^{-1} originating from copper(I) carbonyl. Importantly, the amount of copper(I) carbonyl species corresponds to a maximum of 5 $\mu mol\,g^{-1}$ (Table S5), which is significantly lower as compared to the case of methane conversion and correlates with higher ethylene selectivity in reactor tests. The lower intensity of the band at 2159 cm^{-1} can also be associated with the competitive adsorption of olefins and carbon monoxide for Cu^{I} adsorption center. It is critical that no signals due to other overoxidation products, such as formates, acetates and carbonates, were detected, suggesting only minor overoxidation of ethane in the course of reaction with CuMOR. This is in line with the high selectivity towards ethylene in the reactor (Figure 1E, Table S2). Interestingly, the spectra corresponding to reaction temperatures between 323 and 373 K contain the bands at 2950 cm^{-1} and 1463 cm^{-1} typical of ethanol adsorbed over zeolites.[51] An increase in the reaction temperature to 473 K results in appearance of bands at 1686 cm^{-1} and 1536 cm^{-1} corresponding to acetaldehyde[51] (Table S3). However, there are no signals due to ethanol and acetaldehyde at reaction temperatures above 473 K.

Figure 2C shows the spectra of surface species formed after reaction of propane with CuMOR. All the spectra contain multiple bands corresponding to propylene adsorbed over copper (I) sites (Table S3, Scheme 1C), similarly to ethane conversion. The bands centered at 3062, 2960, 2940, 2922, 2899 and 2866 cm^{-1} are due to C–H stretching vibrations, the band at 1543 cm^{-1} is associated with the C=C vibration, that at 1455 cm^{-1} is the $=CH_2$ scissoring vibration and those at 1438, 1406 and 1380 cm^{-1} are related to the C–H deformation vibrations of propylene.[30,52,53] Additionally, there are signals due to adsorbed water, centered at 1625 cm^{-1} and due to copper(I) carbonyl, centered at 2159 cm^{-1}. Notably, the amount of copper(I) carbonyl species is lower than 4 $\mu mol\,g^{-1}$ (Table S5) and there are no signals characteristic of C_3-oxygynate species, indicating that propane is almost exclusively converted to propylene and water over CuMOR.

Further analysis of the reaction between copper-containing mordenite and different alkanes is based on in situ MAS NMR spectroscopy. The experiments were performed with the samples in a controlled environment and applying the following techniques: ^{13}C high-power proton decoupling (^{13}C HPDEC), ^{1}H-^{13}C cross-polarization (^{1}H-^{13}C CP/MAS) MAS NMR and ^{1}H MAS NMR.[54] The ^{13}C HPDEC method uses single-pulse direct excitation of ^{13}C nuclei. ^{1}H-^{13}C CP/MAS experiment is based on the polarization transfer from ^{1}H to ^{13}C nuclei. It is therefore more sensitive to ^{13}C-containing species with protons in close vicinity under the condition that no averaging of the ^{1}H-^{13}C dipolar interaction occurs because of fast molecular motion. The ^{1}H MAS NMR and ^{1}H-^{13}C CP/MAS spectra are presented in Figure S5 and Figure S6. The assignment of the observed NMR signals is summarized in Table S3. Figure 3A demonstrates the ^{13}C HPDEC MAS NMR spectra after reaction of CuMOR with methane at different temperatures. It contains a very broad signal at −6 ppm, assigned to the carbon atom in molecular methane.[55] The reaction between methane and CuMOR below 498 K leads to the appearance of a signal at 58 ppm due to methoxy species bonded to the zeolite framework[23–25,43,56] (Scheme 1A). At higher reaction temperatures, there are additional signals at 67 ppm and 52 ppm, which are assigned to DME adsorbed over copper(I) sites[24,26,43,57] and molecularly adsorbed methanol,[23–25,43,56] respectively. Furthermore, a weak signal at 174 ppm with asymmetrical side-bands is present in the spectra corresponding to sample reacted at temperatures above 523 K. The signal correspond copper(I) carbonyls[24,43,57,58] formed in methane overoxidation reaction. An additional confirmation for this assignment is the absence of the signal in the ^{1}H-^{13}C CP/MAS NMR spectra (Figure S5), indicating that there are no protons in close vicinity to the corresponding species. Similar to the results of FTIR, the signals due to methoxy species vanish after reaction at temperatures above 623 K.

Figures 3B and C show ^{13}C HPDEC NMR spectra corresponding to the reaction between CuMOR and ethane and propane, respectively. After the adsorption of alkanes, the spectra contain signals at 6 ppm assigned to ethane and at 16 ppm to propane (Table S3). The reaction between CuMOR and ethane starts at 398 K, and leads to the appearance of a signal at 89 ppm with a pronounced spinning sideband pattern separated by the spinning rate of 4 kHz. The intensity of the signals increases with an increase in the reaction temperature, and no other signals are detected within the applied range of reaction temperatures. The values of chemical shift tensor components (Figure S7, Table S5) are characteristic for carbon atoms in ethylene π-complexes with Cu^{I}[43,59,60] (Scheme 1B). For the reaction of

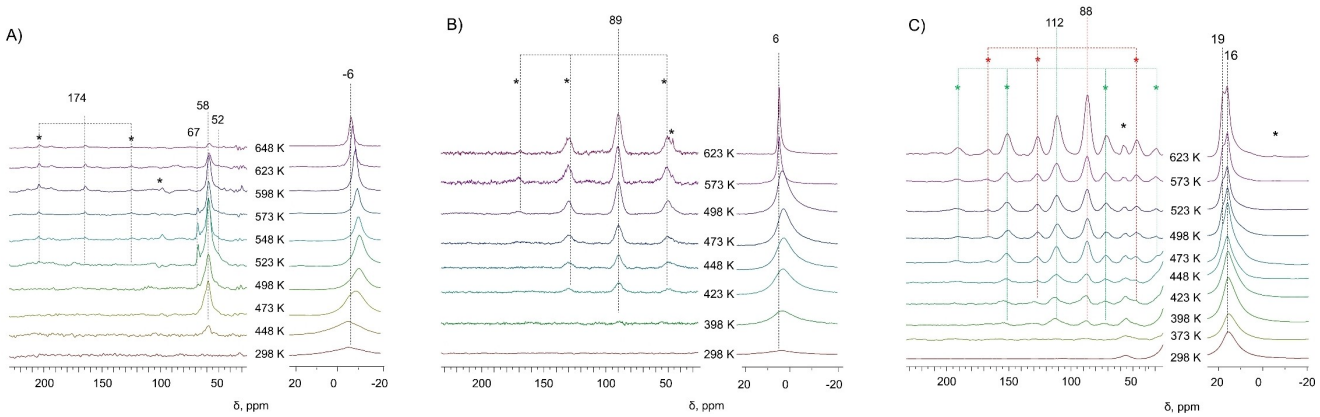

Figure 3. ^{13}C HPDEC spectra after the reaction of CuMOR with methane (A), ethane (B) and propane (C) at different temperatures for 5 minutes. Asterisks denote the spinning side bands.

CuMOR with propane, three signals at 112, 88 and 19 ppm with corresponding spinning sidebands appear at 398 K and develop in the spectra as the reaction temperature increases. These signals are attributed to carbon atoms in CH, CH_2 and CH_3 fragments of propylene adsorbed over copper(I) site, respectively[61] (Tables S3 and S5, Scheme 1C). Additionally, the reaction between ethane and CuMOR at low reaction temperature was studied by means of time-resolved NMR, and Figure S8 shows corresponding ^{1}H-^{13}C CP/ MAS NMR spectra. The only detected signal under these low-conversion conditions at 89 ppm corresponds to ethylene molecule coordinated to Cu^{I} adsorption site, and no other signals were found. In summary, MAS NMR reveals the direct transformation of ethane and propane over CuMOR to ethylene and propylene adsorbed over copper(I) sites without the formation of any other detectable intermediates. Notably, even at 623 K, the adsorbed olefins do not undergo further transformation, such as oligomerization and further oxidation, indicating the high stability of the π-complexes of the olefins and copper(I) centers.

The results of reactor tests and of FTIR and NMR spectroscopies clearly show that the nature of the reaction intermediates varies for different alkanes. Methane activation requires >100 K higher temperature than that ethane and propane, which behave similarly. This behavior indicates that different reaction mechanisms take place. To clarify this suggestion and obtain kinetic information of reaction of CuMOR with different alkanes, the copper reduction was evaluated by means of in situ time-resolved Cu K-edge X-ray absorption spectroscopy (XAS).

Figures 4A–C and Figure S9 show the evolution of Cu K-edge XAS spectra during TPR in methane, ethane and propane. The spectra of the oxygen-activated CuMOR (dark blue lines) contain a weak peak at 8977 eV due to 1s→3d quadrupole transition and a shoulder at 8986 corresponding to 1s→4p transition typical of copper(II) species in CuMOR.[28,62] Upon reaction of CuMOR with alkanes, the intensity of the aforementioned signals decreases and, simultaneously, a signal at 8983 eV appears and develops. The signal is characteristic of 1s→4p transition in copper(I)-containing zeolites[19,28] indicating the reduction of copper (II) sites. Figure 4D illustrates the evolution of the Cu^{II} fraction versus temperature from the MCR-ALS analysis (Section 2.7 of the Supporting Information). Reduction with ethane and propane occurs in a similar manner: the onset of the reduction of Cu^{II} already starts at 350 K, and the maximal rate of reduction estimated as the point of the maximum absolute value of the derivative, is observed at around 500 K. In contrast, temperatures above 400 K are required for the reduction of CuMOR with methane, and the highest rate of reduction occurs at 550 K (Figure 4D). The results show a pronounced difference between the reaction of the copper(II) sites with methane and ethane/ propane and are in line with the recent report by Kvande et al. showing that Cu^{II} reduction with ethane occurs at lower temperature as compared to the reduction with methane.[63]

The kinetics of copper(II) reduction were then evaluated by monitoring the evolution of the Cu K-edge XAS spectra in the course of the isothermal reaction between CuMOR and different alkanes at different temperatures. Figure S10 shows the Cu K-edge XAS spectra, and Figures 5A–C illustrate the corresponding fraction of Cu^{II} evaluated from the linear combination fitting (LCF) analysis. The initial rate of copper reduction was determined from the tangential slope within a reaction period where the Cu^{II} conversion was lower than 10 %, assuming pseudo-zero order for alkanes, which were used in excess. The rates of copper(II) reduction, measured at the same temperature, differ significantly for the various alkanes: reduction with methane is slower by one order of magnitude than it is with the other alkanes. The reduction with propane is only three times faster than that with ethane. Moreover, the effect of the reaction temperature is different for the cases of methane, ethane and propane. The analysis using Arrhenius equation is presented in Figure 5D. An apparent activation energy of $E_a = 61 \pm 7$ kJ mol^{-1} was determined for CuMOR reduction with methane, while the corresponding values for the reduction of CuMOR with ethane and propane were $E_a = 69 \pm 9$ kJ mol^{-1} and $E_a = 68 \pm 5$ kJ mol^{-1}, respectively. The observed differences in the reaction rates and apparent

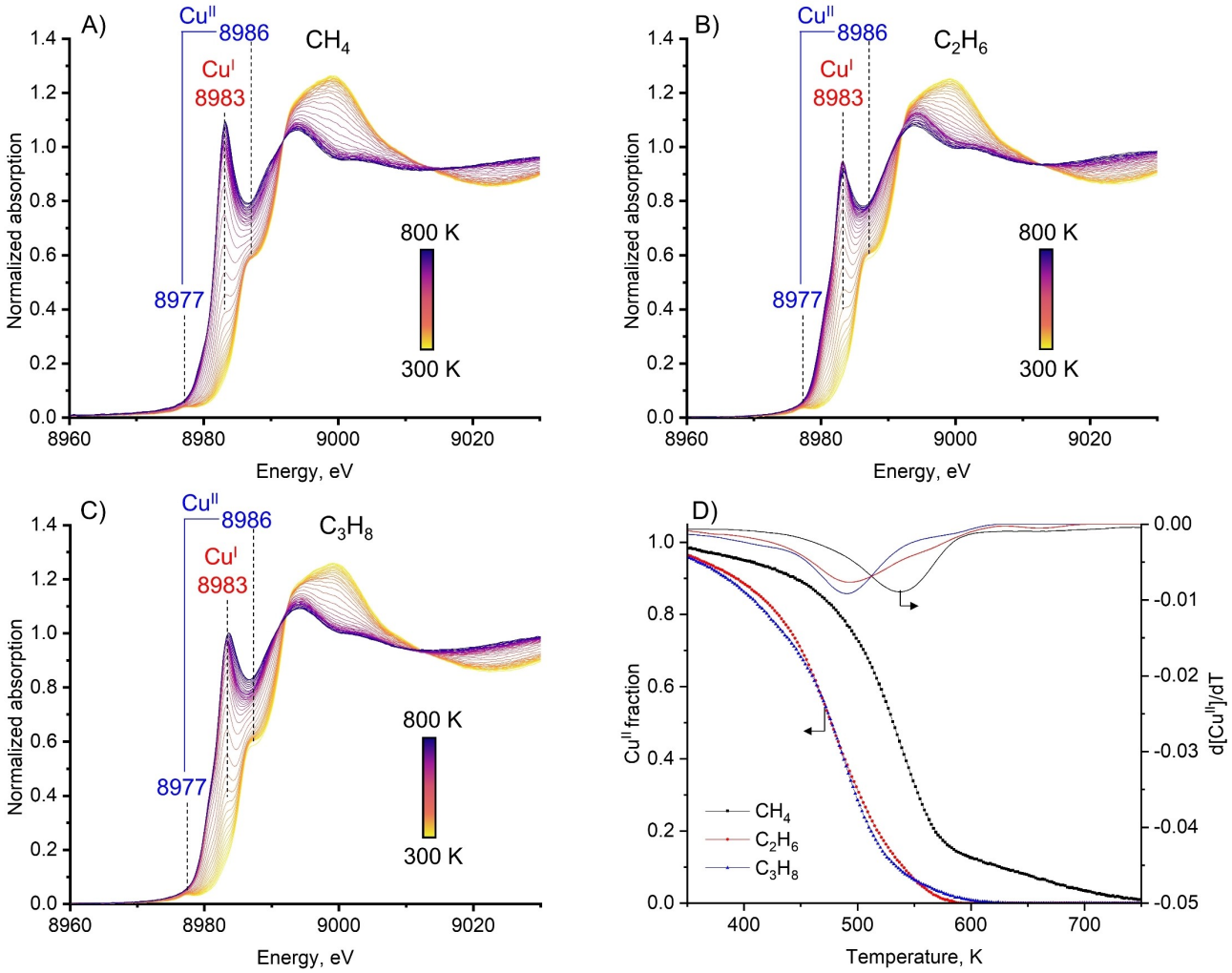

Figure 4. Cu K-edge XANES spectra during the temperature-programmed reduction of CuMOR in methane (A), ethane (B) and propane (C) and fraction of Cu^{II} obtained from MCR-ALS analysis plotted together with its first derivative (D).

activation energies suggest a different mechanism of C–H bond activation for various alkanes.

Oxygen-activated copper-containing mordenite is capable of C–H bond activation in C_1–C_3 alkanes. While the methane conversion to methanol over copper-containing zeolites is well-studied, the activation of ethane and propane is studied much less, and the mechanism of C–H bond activation in these compounds is unclear. We show that the reaction of copper-containing mordenite with ethane and propane differs from methane activation. First, the nature of the formed product is significantly different: ethane and propane are converted to the corresponding olefins, and this process is accompanied by the formation of water. In contrast, in the case of methane conversion, the main products are methanol and dimethyl ether. Moreover, different sites of the copper-containing zeolite participate in the stabilization of partial oxidation products: the reaction of ethane and propane with CuMOR leads to highly stable π-complexes of olefins with copper(I) sites, while oxidation of methane results in the formation of surface methoxy species bonded to the zeolite framework (Scheme 1). Notably, the stabilization of methoxy species is not sufficient to prevent overoxidation at elevated temperatures, as proven by the loss of selectivity in reactor tests (Figure 1) and disappearance of the corresponding signals in FTIR and NMR spectra (Figures 2 and 3). Additionally, the temperature required for the activation of ethane and propane is significantly lower as compared to methane, as revealed by reactor tests (Figure 1), in situ FTIR (Figure 2) and MAS NMR (Figure 3) spectroscopies as well as XAS TPR (Figure 4). Finally, a different apparent activation energy of the reduction of Cu^{II} with different alkanes was observed (Figure 5D). Thus, the reaction with methane has an E_a of about 61 kJ mol^{-1}, and the reduction of Cu^{II} with ethane and propane possesses an apparent activation energy of about 69 kJ mol^{-1}. Although the values differ slightly, very similar values in the case of ethane and propane and by ≈10 kJ mol^{-1} different value for methane suggest different reaction mechanisms. Importantly, the obtained value of ≈60 kJ mol^{-1} for Cu^{II} reduction with methane is typical of the reaction between methane and a mono-μ-oxo dicopper-(II) site[15,64,65] For the case of Cu^{II} reduction with ethane and

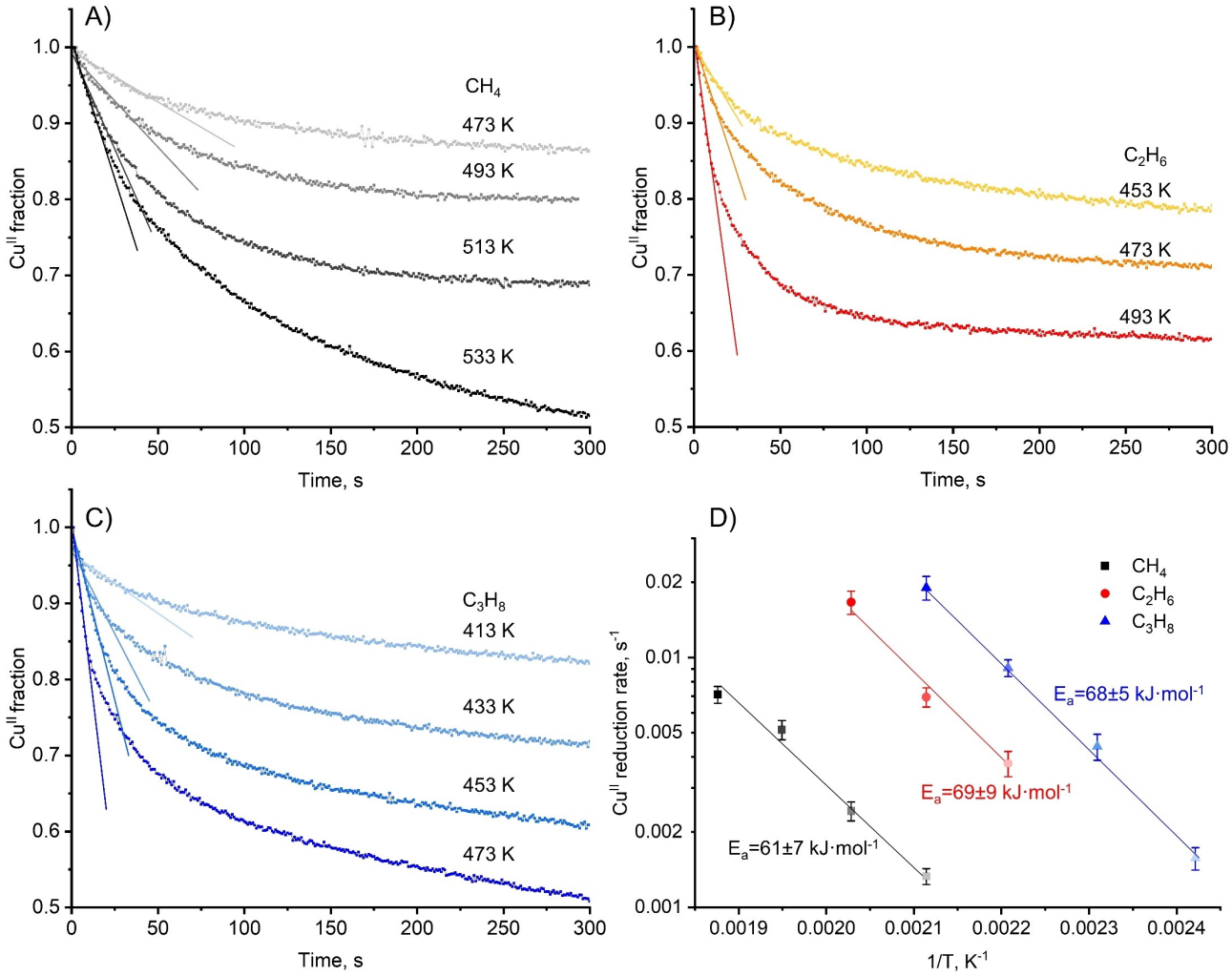

Figure 5. Temporal evolution of the fraction of Cu^{II} during the reaction between CuMOR and methane (A), ethane (B) and propane (C) at different reaction temperatures evaluated from MRC-ALS analysis. The tangent applied for determining the initial rate of reduction are shown. Arrhenius plot for the initial rate of copper reduction (D).

propane the apparent activation energy is close to the reported value for the oxidative dehydrogenation of cyclohexane over a copper oxide catalyst.[66] Taken together, the mentioned observations clearly point to the different mechanisms in the activation of methane and ethane/propane over CuMOR.

Copper-containing mordenite stabilizes mono-μ-oxo dicopper(II) sites,[18,20,64,67] and the proposed mechanism for methane activation over it is presented in Scheme 2A. The reaction leads to the formation of methoxy species, which are stabilized by being bonded to the zeolite framework, hence realizing product protection.[26,68]

We propose two possible pathways for the oxidative dehydrogenation of ethane and propane over mono-μ-oxo dicopper(II) site (Scheme 2B). The first mechanism consists of two consecutive reactions: i) formation of an alkoxy intermediate followed by ii) its rapid conversion to water and olefin-Cu^{I} complex. The second reaction should be much faster than the first one, as suggested by the absence of any substantial amount of alkoxy species by in situ MAS NMR and FTIR spectroscopies (Figures 2 and 3). An alternative mechanism implies a simultaneous abstraction of two hydrogen atoms from the alkane and the formation of water and the olefin-Cu^{I} π-complex. Both mechanisms have been suggested for the oxidative dehydrogenation of alkanes over vanadia-based catalysts.[12,13] For the reaction of ethane with copper(II)-containing mordenite, the formation of a stable ethoxy intermediate, which dehydrates to ethylene, was proposed recently.[31] According to our data (Figure 2B), the corresponding alkoxy intermediates were found only for ethane conversion at temperatures below 423 K (Figure 2B). At the same time, in the conversion of ethane at higher temperature and propane activation in the studied temperature range the only detected products are olefin-Cu^{I} π-complexes. We suggest that the mechanism of direct dehydrogenation with simultaneous abstraction of two hydrogen atoms is more likely above 423 K. The two proposed mechanisms are interconnected, and the corresponding pathways can coexist, but this requires further investigation. ^{1}H MAS NMR (Figure S5) and FTIR of the

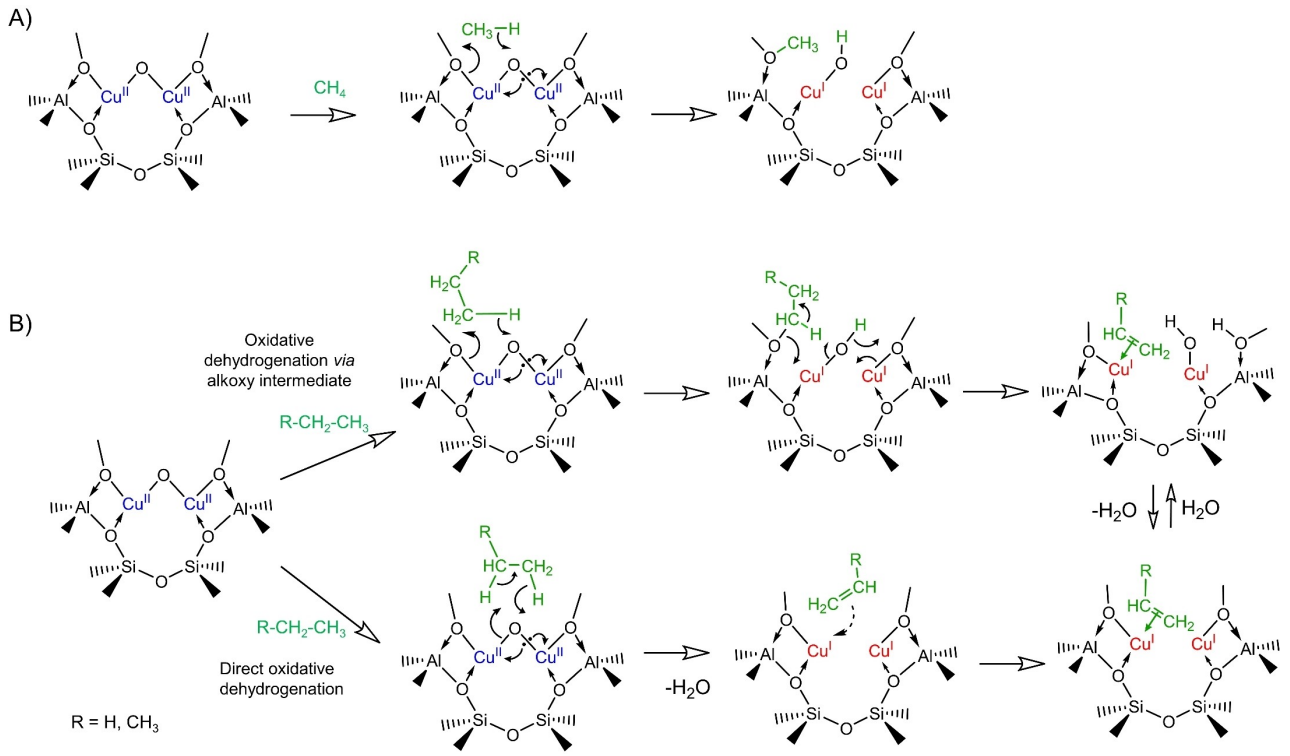

Scheme 2. Proposed reaction mechanisms for methane oxidation to methoxy species (A) and oxidative dehydrogenation of ethane or propane with formation of π-complex between olefin and Cu^{I} (B) over mono-μ-oxo dicopper(II) site hosted in the zeolite framework. Carbon-containing reactants and products are shown in green, copper atoms in "+2" and "+1" oxidation states are shown in blue and red, respectively.

OH-region (Figure S4) show that the conversion of ethane and propane results in the appearance of a signal at 4.1 ppm and a band at 3615 cm^{-1} due to the formation of Brønsted acid sites.[69] We suggest that the formed water can participate in the hydrolysis of the Cu^{I}-O–Al bond leading to the formation of $Cu^{I}OH$ species and the above-mentioned Brønsted acid sites (Scheme 2B). However, establishing of the precise structure of copper(I) species requires additional investigation. The weak signal due to ethanol and acetaldehyde in FTIR spectra corresponding to ethane oxidation at 323 K and 373 K (Figure 2B) might indicate that the ethoxy species formed during ethane conversion are transformed to ethanol, which is oxidized to acetaldehyde. However, it also may be the case that ethanol is formed via ethylene hydration.[70] Both of the two proposed mechanisms of reaction between alkane and copper-containing zeolite imply that the main product is a π-complex between olefin and copper(I), rather than surface alkoxy species.[31] We show that the strong adsorption of olefin over copper(I) prevents it from further oxidation or oligomerization, hence realizing product protection.

The last step in the chemical looping process is exposure of the reacted material to a water-containing gas phase to desorb the products. For ethane and propane, exposure to water results in the desorption of the olefins from the π-complex with copper(I) due to its decomposition via the competitive water adsorption. Thus, water-assisted desorption enables the direct release of gaseous olefins, hence making the standard chemical looping protocol applicable for the conversion of ethane and propane to ethylene and propylene. Further detailed studying of the decomposition mechanism can aid in optimizing the olefins desorption step. Importantly, the chemical processes taking place during the olefins release to the gas phase are significantly different to the desorption step in the methane to methanol process, where hydrolysis of surface methoxy species must take place for the formation of methanol and dimethyl ether.[29,56]

Conclusion

Copper(II)-containing mordenite enables activation of the C–H bond in C_1-C_3 alkanes, and the mechanism and reaction chemistry is different for ethane/propane and methane. Ethane and propane undergo oxidative dehydrogenation and are transformed into corresponding olefins strongly adsorbed over copper(I) species. The formation of these strong π-complexes protects olefins from further over-oxidation and oligomerization, enabling high selectivity. Even in a non-optimized system, the selectivity of above 95 % towards ethylene and above 85 % towards propylene is obtained. Upon contact with water under mild conditions, the formed π-complexes decompose to free olefins. This differs from the activation of methane, which occurs via oxidative hydroxylation and results in the formation of methoxy species attached to the zeolite framework, which need to be hydrolyzed to methanol/dimethyl ether upon contact with water. The results provide insights in C–H

bond activation chemistry at the molecular level and show a novel potential application of copper-containing zeolites for effective valorization of the short-chain alkanes.

Acknowledgements

We acknowledge the assistance of Mr. Andreas Brenig and Mr. Jörg Fischer during XAS measurements at SuperXAS beamline. V.L.S. and J.A.v.B thank the Energy System Integration platform of the Paul Scherrer Institute for financial support. J.A.v.B. and M.A.A. thank the SNF for financial support, project 200021_178943. Open Access funding provided by Eidgenössische Technische Hochschule Zürich.

Conflict of Interest

The authors declare no conflict of interest.

Data Availability Statement

The data that support the findings of this study are available from the corresponding author upon reasonable request.

Keywords: Copper Zeolites · Dehydrogenation · Oxidation · Reaction Mechanisms

[1] J. A. Labinger, J. E. Bercaw, *Nature* **2002**, *417*, 507–514.
[2] Y. Wang, P. Hu, J. Yang, Y. A. Zhu, D. Chen, *Chem. Soc. Rev.* **2021**, *50*, 4299–4358.
[3] S. Faramawy, T. Zaki, A. A. E. Sakr, *J. Nat. Gas Sci. Eng.* **2016**, *34*, 34–54.
[4] J. R. Rostrup-Nielsen, J. Sehested, J. K. Nørskov, *Adv. Catal.* **2002**, *47*, 65–139.
[5] M. E. Dry, *J. Chem. Technol. Biotechnol.* **2002**, *77*, 43–50.
[6] J. P. Lange, *Catal. Today* **2001**, *64*, 3–8.
[7] K. Aasberg-Petersen, I. Dybkjær, C. V. Ovesen, N. C. Schjødt, J. Sehested, S. G. Thomsen, *J. Nat. Gas Sci. Eng.* **2011**, *3*, 423–459.
[8] J. H. Lunsford, *Catal. Today* **2000**, *63*, 165–174.
[9] Z. Gholami, F. Gholami, Z. Tišler, M. Vakili, *Energies* **2021**, *14*, 8190.
[10] T. Ren, M. Patel, K. Blok, *Energy* **2006**, *31*, 425–451.
[11] E. A. Mamedov, V. Cortés Corberán, *Appl. Catal. A* **1995**, *127*, 1–40.
[12] S. Chen, X. Chang, G. Sun, T. Zhang, Y. Xu, Y. Wang, C. Pei, J. Gong, *Chem. Soc. Rev.* **2021**, *50*, 3315–3354.
[13] R. Grabowski, *Catal. Rev. Sci. Eng.* **2006**, *48*, 199–268.
[14] "Telehealth Market Size to Hit USD 224.8 Billion by 2030," can be found under https://www.precedenceresearch.com/telehealth-market, **n.d**.
[15] M. H. Groothaert, P. J. Smeets, B. F. Sels, P. A. Jacobs, R. A. Schoonheydt, *J. Am. Chem. Soc.* **2005**, *127*, 1394–1395.
[16] M. A. Newton, A. J. Knorpp, V. L. Sushkevich, D. Palagin, J. A. Van Bokhoven, *Chem. Soc. Rev.* **2020**, *49*, 1449–1486.
[17] N. F. Dummer, D. J. Willock, Q. He, M. J. Howard, R. J. Lewis, G. Qi, S. H. Taylor, J. Xu, D. Bethell, C. J. Kiely, G. J. Hutchings, *Chem. Rev.* **2023**, *123*, 6359–6411.
[18] V. L. Sushkevich, O. V. Safonova, D. Palagin, M. A. Newton, J. A. van Bokhoven, *Chem. Sci.* **2020**, *11*, 5299–5312.
[19] G. Deplano, A. Martini, M. Signorile, E. Borfecchia, V. Crocellà, S. Svelle, S. Bordiga, *Angew. Chem. Int. Ed.* **2021**, *60*, 25891–25896.
[20] D. K. Pappas, A. Martini, M. Dyballa, K. Kvande, S. Teketel, K. A. Lomachenko, R. Baran, P. Glatzel, B. Arstad, G. Berlier, C. Lamberti, S. Bordiga, U. Olsbye, S. Svelle, P. Beato, E. Borfecchia, *J. Am. Chem. Soc.* **2018**, *140*, 15270–15278.
[21] M. A. Artsiusheuski, J. A. van Bokhoven, V. L. Sushkevich, *J. Phys. Chem. C* **2021**, *125*, 26512–26521.
[22] G. Brezicki, J. Zheng, C. Paolucci, R. Schlögl, R. J. Davis, *ACS Catal.* **2021**, *11*, 4973–4987.
[23] M. Dyballa, K. Thorshaug, D. K. Pappas, E. Borfecchia, K. Kvande, S. Bordiga, G. Berlier, A. Lazzarini, U. Olsbye, P. Beato, S. Svelle, B. Arstad, *ChemCatChem* **2019**, *11*, 5022–5026.
[24] V. L. Sushkevich, R. Verel, J. A. Bokhoven, *Angew. Chem. Int. Ed.* **2020**, *59*, 910–918.
[25] A. A. Kolganov, A. A. Gabrienko, S. A. Yashnik, E. A. Pidko, A. G. Stepanov, *ACS Appl. Mater. Interfaces* **2020**, *124*, 6242–6252.
[26] M. A. Artsiusheuski, R. Verel, J. A. van Bokhoven, V. L. Sushkevich, *ACS Catal.* **2021**, *11*, 12543–12556.
[27] M. A. Newton, A. J. Knorpp, A. B. Pinar, V. L. Sushkevich, D. Palagin, J. A. Van Bokhoven, *J. Am. Chem. Soc.* **2018**, *140*, 10090–10093.
[28] M. A. Artsiusheuski, O. Safonova, D. Palagin, J. A. van Bokhoven, V. L. Sushkevich, *J. Phys. Chem. C* **2023**, *127*, 9603–9615.
[29] N. V. Beznis, B. M. Weckhuysen, J. H. Bitter, *Catal. Lett.* **2010**, *138*, 14–22.
[30] K. Horiguchi, A. Itadani, K. Uematsu, K. Toda, M. Sato, *Vib. Spectrosc.* **2020**, *106*, 103016.
[31] K. Kvande, S. Prodinger, B. G. Solemsli, S. Bordiga, E. Borfecchia, U. Olsbye, P. Beato, S. Svelle, *Chem. Commun.* **2023**, *59*, 6052–6055.
[32] M. Ahlquist, R. J. Nielsen, R. A. Periana, W. A. Goddard, *J. Am. Chem. Soc.* **2009**, *131*, 17110–17115.
[33] J. P. Lange, V. L. Sushkevich, A. J. Knorpp, J. A. Van Bokhoven, *Ind. Eng. Chem. Res.* **2019**, *58*, 8674–8680.
[34] Z. R. Jovanovic, J. P. Lange, M. Ravi, A. J. Knorpp, V. L. Sushkevich, M. A. Newton, D. Palagin, J. A. van Bokhoven, *J. Catal.* **2020**, *385*, 238–245.
[35] V. L. Sushkevich, D. Palagin, M. Ranocchiari, J. A. Van Bokhoven, *Science* **2017**, *356*, 523–527.
[36] V. L. Sushkevich, J. A. Van Bokhoven, *Catal. Sci. Technol.* **2020**, *10*, 382–390.
[37] A. A. Guda, S. A. Guda, K. A. Lomachenko, M. A. Soldatov, I. A. Pankin, A. V. Soldatov, L. Braglia, A. L. Bugaev, A. Martini, M. Signorile, E. Groppo, A. Piovano, E. Borfecchia, C. Lamberti, *Catal. Today* **2019**, *336*, 3–21.
[38] D. K. Pappas, E. Borfecchia, M. Dyballa, I. A. Pankin, K. A. Lomachenko, A. Martini, M. Signorile, S. Teketel, B. Arstad, G. Berlier, C. Lamberti, S. Bordiga, U. Olsbye, K. P. Lillerud, S. Svelle, P. Beato, *J. Am. Chem. Soc.* **2017**, *139*, 14961–14975.
[39] H. J. Bernstein, *Trans. Faraday Soc.* **1962**, *58*, 2285–2306.
[40] V. L. Sushkevich, J. A. Van Bokhoven, *ACS Catal.* **2019**, *9*, 6293–6304.
[41] T. R. Forester, R. F. Howe, *J. Am. Chem. Soc.* **1987**, *109*, 5076–5082.
[42] X. Z. Jiang, *J. Mol. Catal. A* **1997**, *121*, 63–68.
[43] M. A. Artsiusheuski, R. Verel, J. A. van Bokhoven, V. L. Sushkevich, *ACS Catal.* **2023**, *13*, 5864–5875.
[44] E. Kukulska-Zaja¸c, J. Datka, *J. Phys. Chem. C* **2007**, *111*, 3471–3475.

[45] M. A. Artsiusheuski, J. A. Van Bokhoven, V. L. Sushkevich, *ACS Catal.* **2022**, *12*, 15626–15637.
[46] J. W. Ward, *J. Phys. Chem.* **1968**, *72*, 4211–4223.
[47] F. X. Llabrés i Xamena, P. Fisicaro, G. Berlier, A. Zecchina, G. T. Palomino, C. Prestipino, S. Bordiga, E. Giamello, C. Lamberti, *J. Phys. Chem. B* **2003**, *107*, 7036–7044.
[48] G. Deplano, M. Signorile, V. Crocellà, N. G. Porcaro, C. Atzori, B. G. Solemsli, S. Svelle, S. Bordiga, *ACS Appl. Mater. Interfaces* **2022**, *14*, 21059–21068.
[49] M. Li, J. Shen, *Mater. Chem. Phys.* **2001**, *68*, 204–209.
[50] E. Broclawik, P. Kozyra, J. Datka, *C. R. Chim.* **2005**, *8*, 491–508.
[51] Ł. Kuterasiński, J. Podobiński, J. Datka, *Molecules* **2021**, *26*, 2669.
[52] F. Benaliouche, Y. Boucheffa, F. Thibault-Starzyk, *Microporous Mesoporous Mater.* **2012**, *147*, 10–16.
[53] T. E. Hoost, K. A. Laframboise, K. Otto, *Appl. Catal. B* **1995**, *7*, 79–93.
[54] A. E. Bennett, C. M. Rienstra, M. Auger, K. V. Lakshmi, R. G. Griffin, *J. Chem. Phys.* **1995**, *103*, 6951–6958.
[55] G. M. Bowers, H. T. Schaef, Q. R. S. Miller, E. D. Walter, S. D. Burton, D. W. Hoyt, J. A. Horner, J. S. Loring, B. P. McGrail, R. J. Kirkpatrick, *ACS Earth Space Chem.* **2019**, *3*, 324–328.
[56] Y. Jiang, M. Hunger, W. Wang, *J. Am. Chem. Soc.* **2006**, *128*, 11679–11692.
[57] L. Zhou, S. Li, G. Qi, Y. Su, J. Li, A. Zheng, X. Yi, Q. Wang, F. Deng, *Solid State Nucl. Magn. Reson.* **2016**, *80*, 1–6.
[58] A. V. Yakimov, V. L. Sushkevich, J. A. Van Bokhoven, C. Copéret, *J. Phys. Chem. C* **2022**, *126*, 3681–3687.
[59] R. M. Sullivan, H. Liu, D. S. Smith, J. C. Hanson, D. Osterhout, M. Ciraolo, C. P. Grey, J. D. Martin, *J. Am. Chem. Soc.* **2003**, *125*, 11065–11079.
[60] S. Halbert, C. Copéret, C. Raynaud, O. Eisenstein, *J. Am. Chem. Soc.* **2016**, *138*, 2261–2272.
[61] Z. N. Lashchinskaya, A. A. Gabrienko, A. G. Stepanov, *Microporous Mesoporous Mater.* **2023**, *350*, 112448.
[62] C. Lamberti, S. Bordiga, M. Salvalaggio, G. Spoto, A. Zecchina, F. Geobaldo, G. Vlaic, M. Bellatreccia, *J. Phys. Chem. B* **1997**, *101*, 344–360.
[63] K. Kvande, B. Garetto, G. Deplano, M. Signorile, B. G. Solemsli, S. Prodinger, U. Olsbye, P. Beato, S. Bordiga, S. Svelle, E. Borfecchia, *Chem. Sci.* **2023**, https://doi.org/10.1039/D3SC01677 C.
[64] V. L. Sushkevich, M. Artsiusheuski, D. Klose, G. Jeschke, J. A. van Bokhoven, *Angew. Chem. Int. Ed.* **2021**, *60*, 15944–15953.
[65] J. S. Woertink, P. J. Smeets, M. H. Groothaert, M. A. Vance, B. F. Sels, R. A. Schoonheydt, E. I. Solomon, *Proc. Natl. Acad. Sci. USA* **2009**, *106*, 18908–18913.
[66] S. L. Nauert, F. Schax, C. Limberg, J. M. Notestein, *J. Catal.* **2016**, *341*, 180–190.
[67] E. Borfecchia, D. K. Pappas, M. Dyballa, K. A. Lomachenko, C. Negri, M. Signorile, G. Berlier, *Catal. Today* **2019**, *333*, 17–27.
[68] D. K. Pappas, E. Borfecchia, K. A. Lomachenko, A. Lazzarini, E. S. Gutterød, M. Dyballa, A. Martini, G. Berlier, S. Bordiga, C. Lamberti, B. Arstad, U. Olsbye, P. Beato, S. Svelle, *Top. Catal.* **2019**, *62*, 712–723.
[69] L. Heeribout, V. Semmer, P. Batamack, C. Dorémieux-Morin, R. Vincent, J. Fraissard, *Stud. Surf. Sci. Catal.* **1996**, *101*, 831–840.
[70] N. Katada, Y. Iseki, A. Shichi, N. Fujita, I. Ishino, K. Osaki, T. Torikai, M. Niwa, *Appl. Catal. A* **2008**, *349*, 55–61.

Manuscript received: June 29, 2023
Accepted manuscript online: September 12, 2023
Version of record online: September 22, 2023